ORNL/CP-102362

IMPROVING THE ACCURACY OF HIGH-ORDER NODAL TRANSPORT METHODS

O. M. Zamonsky and G. C. Buscaglia
Centro Atomico Bariloche and Instituto Balseiro
8400- Bariloche, RN, Agentina
zamonsky@cab.cnea.gov.ar; gustavo@cab.cnea.gov.ar

Y. Y. Azmy
*Oak Ridge National Laboratory**
P.O. Box 2008, MS-6363
Oak Ridge, Tennessee 37831-6363
Phone: (423) 574-8069 Fax: (423) 574-9619
yya@ornl.gov

Full paper submitted for review, American Nuclear Society's International Conference on Mathematics and Computation, Reactor Physics and Environmental Analysis in Nuclear Applications, Madrid, Spain, September 27–30, 1999.

---

*Research sponsored by the Oak Ridge National Laboratory managed by Lockheed Martin Energy Research Corporation for the U.S. Department of Energy under contract No. DE-AC05-96OR22464.

Improving the Accuracy of High-Order Nodal Transport Methods

O. M. Zamonsky and G. C. Buscaglia
Centro Atómico Bariloche and Instituto Balseiro
8400- Bariloche, RN, Argentina
zamonsky@cab.cnea.gov.ar ; gustavo@cab.cnea.gov.ar

Y. Y. Azmy
Oak Ridge National Laboratory
Oak Ridge, Tennessee 37831-6363, USA
yya@ornl.gov

Abstract

This paper outlines some recent advances towards improving the accuracy of neutron transport calculations using the Arbitrarily High Order Transport-Nodal (AHOT-N) Method. These advances consist of several contributions: (a) A formula for the spatial weights that allows for the polynomial order to be raised arbitrarily high without suffering from pollution from round-off error; (b) A reconstruction technique for the angular flux, based upon a recursive formula, that reduces the pointwise error by one order; (c) An *a posteriori* error indicator that estimates the true error and its distribution throughout the domain, so that it can be used for adaptively refining the approximation. Present results are mainly for 1D, extension to 2D-3D is in progress.

Introduction

The Arbitrarily High-Order Nodal (AHOT-N) method in the final form proposed by Azmy, (Azmy, 1988) was shown to be a computationally efficient way of obtaining highly accurate approximations to neutron transport problems. In the last few years, some progress has been made towards improving the accuracy of this method. The final goal, not yet accomplished, is a rigorously-based numerical methodology capable of achieving arbitrary accuracy with automatic error control. This paper presents our overviews of recent advances from the viewpoint of this goal.

The AHOT-N method is based on an expansion of the external source and the scattering term inside each cell in polynomials of degree lower than or equal to some user-defined value Λ. A brief review of AHOT-N is presented in Section 2. The numerical solution, which we denote by $\underline{\psi}$, consists within each cell of a polynomial part of order Λ, denoted by $\underline{\tilde{\psi}}$, plus a correction that is usually computed only at cell interfaces. The *a priori* convergence properties of the AHOT-N method in 1D result from the analysis of so-called exact moment methods by Victory and Ganguly (Victory, 1986) (see also (Nelson, 1987) and (Keller, 1988), and references cited therein). It is shown that $\underline{\psi}$ converges to the exact solution as $h^{\Lambda+2}$, with superconvergence (as $h^{2\Lambda+2}$) at cell interfaces, where h is the cell size. On the other hand, $\underline{\tilde{\psi}}$ converges as $h^{\Lambda+1}$. To our knowledge, the higher accuracy of $\underline{\psi}$ to get pointwise values of the flux has not been exploited, perhaps because it was considered expensive to evaluate. In Section 3 we present a recursive formula for $\underline{\psi}$ that renders its evaluation inexpensive, and illustrate the gain in accuracy obtained.

This improvement in accuracy, however, can be hindered by round-off errors when Λ is high. To tackle this difficulty, asymptotic limits for the method's coefficients are needed. These were first derived in (Azmy, 1998) and are briefly recalled in Section 4. With this improvement, no restriction is left on Λ, which can in fact be chosen arbitrarily for each calculation cell. Of course, in practical situations such choice is better handled by an automatic adaptive scheme guided by cellwise error indicators.

Rigorous adaptive schemes are based on *a posteriori* error estimators. The first such estimator for the 1D AHOT-N method has been recently derived by the authors in (Zamonsky, 1999). The basic result is that the difference in scattering sources arising from $\underline{\psi}$ and $\underline{\tilde{\psi}}$ estimates the true error distribution. The estimator is recalled in Section 5, which also reports on a further validation of the estimator in a stringent S4 heterogeneous problem.

The results reviewed in this paper are encouraging. Extracting full accuracy with optimal cost in neutron transport calculations is certainly needed to achieve reliable predictions in complex 3D configurations.

2 The AHOT-N Method

2.1 Preliminaries

The discrete-ordinates approximation to the neutron transport equation is given by

$$\mu_i \frac{d\psi_i^e}{dx}(x) + \sigma(x)\psi_i^e(x) = c(x)\sigma(x)\sum_{j=1}^{N} w_j k_{ji}(x)\psi_j^e(x) + q_i(x) \tag{1}$$

with boundary conditions $\psi_i^e(0) = 0$, $\mu_i > 0$, and $\psi_i^e(L) = 0$, $\mu_i < 0$, where $k_{ji}(x)$ is the scattering kernel. Each direction is defined by the quadrature points μ_i, ($\mu_i \neq 0$), $i = 1,\ldots,N$, with associated weights w_i; $\psi_i^e(x)$ are the exact angular fluxes and $q_i(x)$ the external source.
Defining the following NxN matrices

$$\underline{\underline{\mu}} \equiv \begin{bmatrix} \mu_1 & & & \\ & \mu_2 & & \\ & & \cdot & \\ & & & \mu_N \end{bmatrix}, \quad \underline{\underline{S}}(x) \equiv c(x) \begin{bmatrix} w_1k_{11}(x) & w_2k_{21}(x) & \cdot & w_Nk_{N1}(x) \\ w_1k_{12}(x) & w_2k_{22}(x) & \cdot & w_Nk_{N2}(x) \\ \cdot & \cdot & \cdot & \cdot \\ w_1k_{1N}(x) & w_2k_{2N}(x) & \cdot & w_Nk_{NN}(x) \end{bmatrix}, \tag{2}$$

and the vectors

$$\underline{\psi}^e(x) \equiv \begin{bmatrix} \psi_1^e(x) \\ \cdot \\ \psi_N^e(x) \end{bmatrix}, \quad \underline{q}(x) \equiv \begin{bmatrix} q_1(x) \\ \cdot \\ q_N(x) \end{bmatrix}, \tag{3}$$

equation (1) can be written in the following form:

$$\underline{\underline{\mu}} \frac{d\underline{\psi}^e}{dx}(x) + \sigma(x)\underline{\psi}^e(x) = \sigma(x)\underline{\underline{S}}(x)\underline{\psi}^e(x) + \underline{q}(x), \tag{4}$$

Let us now briefly describe the numerical methodology. Assume that the domain $[0, L]$ is decomposed into a finite number of non-overlapping cells $\{C_k, k = 1,..., K\}$. If we assume that σ and $\underline{\underline{S}}$ are constants in each cell, Eq. (4) can be easily solved whenever the right hand side is a polynomial within each cell. Based upon this idea, the AHOT-N method defines a numerical solution $\underline{\psi}$ as the (unique) function that satisfies

$$\underline{\underline{\mu}}\frac{d\underline{\psi}}{dx}(x) + \sigma(x)\underline{\psi}(x) = \sigma(x)\underline{\underline{S}}(x)\underline{\tilde{\psi}}(x) + \underline{\tilde{q}}(x), \tag{5}$$

with the same boundary conditions as $\underline{\psi}^e$.

In Eq. (5), $\underline{\psi}$ depends on the position and on Λ because $\underline{\tilde{\psi}}$ and $\underline{\tilde{q}}$ are defined as the truncated Legendre polynomial expansions of $\underline{\psi}$ and $\underline{q}$, respectively, up to order Λ within each cell C_k. Let us clarify this definition for, e.g., the case of $\underline{\psi}$. Let x be arbitrary and let C_k be the cell containing x. If h_k is the length of C_k and x_k its midpoint, the normalized Legendre polynomial of degree λ in C_k is given by

$$p_{\lambda,k}(x) = p_\lambda\left(2/h_k(x - x_k)\right), \tag{6}$$

where p_λ is the Legendre polynomial of degree λ defined in the interval $[-1,1]$. Now, as the i^{th} component of $\underline{\psi}$ at x can be represented by

$$\psi_i(x) = \sum_{\lambda=0}^{\infty}(2\lambda+1)\psi_{i,(\lambda,k)}p_{\lambda,k}(x), \tag{7}$$

where $\psi_{i,(\lambda,k)}$ are the moments given by

$$\psi_{i,(\lambda,k)} = \frac{1}{h_k}\int_{x_k-h_k/2}^{x_k+h_k/2}\psi_i(x')p_{\lambda,k}(x')dx', \tag{8}$$

we obtain as definition of $\tilde{\psi}_i$,

$$\psi_i(x) = \sum_{\lambda=0}^{\Lambda}(2\lambda+1)\psi_{i,(\lambda,k)}p_{\lambda,k}(x). \tag{9}$$

Notice that Eq. (5) defines $\underline{\psi}$ as the angular fluxes that, upon application of the streaming operator $\underline{\underline{\mu}}\frac{d}{dx} + \sigma$, coincides with the truncated scattering + external sources. Except for the truncation operation, the exact solution $\underline{\psi}^e$ satisfies the same equality (streaming = scattering + external source). This makes $\underline{\psi}$ as obtained from the AHOT-N method, extremely accurate as will be illustrated later on.

2.2 The Weighted-Diamond Difference (WDD) form of the AHOT-N method

Azmy (Azmy, 1988) proposed a WDD equation that relates the values of $\underline{\psi}$ at the extreme points of C_k, $\underline{\psi}(x_{k\pm1/2})=\underline{\psi}(x_k \pm h_k/2)$ to the moments $\underline{\psi}_{(\lambda,k)}, \lambda=1,...,\Lambda$, in a way that depends on a single spatial weight coefficient per discrete ordinate $i=1,...,N$. This formulation implies no additional approximation, so that Eq. (5) remains valid, but greatly alleviates the computational burden so that N, K and Λ can be given large values, improving the approximation, at affordable memory and CPU cost. The interested reader may consult (Azmy, 1988) for the derivation, the final form being:

$$\left(\frac{1+\alpha_\Lambda(t_{i,k})}{2}\right)\psi_i(x_{k+1/2})+\left(\frac{1-\alpha_\Lambda(t_{i,k})}{2}\right)\psi_i(x_{k-1/2})=\sum_{\substack{\lambda=0\\ even}}^{\Lambda}(2\lambda+1)\psi_{i,(\lambda,k)}+\sum_{\substack{\lambda=1\\ odd}}^{\Lambda}(2\lambda+1)\alpha_\Lambda(t_{i,k})\psi_{i,(\lambda,k)}, \quad (10)$$

where $t_{i,k}=\sigma_k h_k/2\mu_i$ is the optical thickness. The spatial weights are given by

$$\alpha_\Lambda(t_{i,k})=\frac{\cosh(t_{i,k})-\sum_{\lambda=0,even}^{\Lambda}e_\lambda(t_{i,k})}{\sinh(t_{i,k})-\sum_{\lambda=1,odd}^{\Lambda}e_\lambda(t_{i,k})}, \quad (11)$$

and $e_\lambda(t_{i,k})\equiv\frac{(2\lambda+1)}{2}\int_{-1}^{1}\exp(t_{i,k}x)p_\lambda(x)dx$.

Equation (10) is supplemented with the moments balance equations,

$$\frac{\mu_i}{h_k}\left\{\psi_i(x_{k+1/2})-(-1)^\lambda\psi_i(x_{k-1/2})-2\sum_{r=0}^{[(\lambda-1)/2]}(2\lambda-4r-1)\psi_{i,(\lambda-2r-1,k)}\right\} \quad (12)$$
$$+\sigma_k\psi_{i,(\lambda,k)}=Q_{i,(\lambda,k)}, \lambda=0,...,\Lambda, i=1,...,N$$

where $Q_{i,(\lambda,k)}$ is the (λ,k) moment of the source for component i.

3. Evaluation and Accuracy Assessment of $\underline{\psi}$

3.1 Pointwise evaluation of $\underline{\psi}$ at an arbitrary point x

As can be seen from the final equations that implement the method (Eqs. 10-12), the computational unknowns are the values of $\underline{\psi}$ at cell interfaces and the moments of $\underline{\psi}$ up to order Λ. When evaluating the numerical solution at some point x, it is thus immediate to compute $\tilde{\underline{\psi}}(x)$ but some extra coding is required to compute $\underline{\psi}(x)$ unless x coincides with a cell interface. However, it can be shown [Victory&Ganguly] that $\underline{\psi}(x)$ converges to the exact solution with an asymptotic order of $h^{\Lambda+2}$, one power of h greater than that of $\tilde{\underline{\psi}}(x)$, whose asymptotic order is $h^{\Lambda+1}$. Moreover, $\underline{\psi}(x)$ is superconvergent as $h^{2\Lambda+2}$ at cell interfaces.

The previous considerations stress the importance of calculating $\underline{\psi}(x)$ any time a pointwise estimation of the angular fluxes is required. Notice that this is a post-processing step, i.e., Eqs. 10-12 are assumed solved by the main code for the computational unknowns. There are mainly two ways of performing this evaluation: (a) The moments of order $\lambda>\Lambda$ can be calculated by taking moments of Eq. 5, or, (b) the pointwise value $\underline{\psi}(x)$ can be obtained by exactly solving Eq. 5 from the adjacent

cell interface, where $\underline{\psi}$ is available, up to point x. Though further research is in progress, alternative (a) worked far worse than alternative (b) in some preliminary tests. We give below the final expressions used for the evaluation of $\underline{\psi}(x)$. Defining

$$\tilde{Q}_i(x) \equiv \sigma(x)\left[\underline{\underline{S}}(x)\underline{\tilde{\psi}}(x)\right]_i + \tilde{q}_i(x), \tag{13}$$

the exact solution of Eq. 5 for $\mu_i > 0$, integrated from the adjacent interface to x is

$$\psi_i(x) = \psi_i(x_{k-1/2}) e^{-\sigma_k (x - x_{k-1/2})/\mu_i} + \frac{1}{\mu_i} \int_{x_{k-1/2}}^{x} e^{-\sigma_k (x-x')/\mu_i} \tilde{Q}_i(x')dx', \quad x \in C_k, \; i = 1,...,N, \tag{14}$$

Expanding $\tilde{Q}$ in Legendre polynomials yields

$$\psi_i(x) = \psi_i(x_{k-1/2}) e^{-\sigma_k (x - x_{k-1/2})/\mu_i} + \frac{1}{\mu_i} \sum_{\lambda=0}^{\Lambda} (2\lambda+1) Q_{i(\lambda,k)} I_{i(\lambda,k)}(x), \quad x \in C_k, \; i = 1,...,N, \tag{15}$$

where

$$I_{i(\lambda,k)}(x) \equiv \int_{x_{k-1/2}}^{x} e^{-\sigma_k (x-x')/\mu_i} p_{\lambda,k}(x')dx'. \tag{16}$$

After some algebra, one arrives at

$$I_{i(\lambda,k)}(x) = \frac{\mu_i}{\sigma_k} \left(p_{\lambda,k}(x) - (-1)^{\lambda} e^{-\sigma_k (x - x_{k-1/2})/\mu_i} - \frac{2}{h_k} \sum_{l=0,1^*}^{\lambda-1} (2l+1) I_{i(l,k)} \right). \tag{17}$$

where $l = 0, 1^*$ indicates that $l = 0$ if λ is odd, $l = 1$ if λ is even, and that the increment in the index of the sum is equal to two. This is a recursive expression that allows the evaluation of $I_{i(\lambda,k)}(x), \lambda = 0,...,\Lambda$, which inserted into Eq. 15 gives the values of $\psi_i(x)$ for $\mu_i > 0$. The expression for $\mu_i < 0$ is obtained analogously.

3.2 Numerical assessment

We implemented the 1D, AHOT-N method in a discrete-ordinates steady-state code for solving monoenergetic, fixed source, isotropic scattering problems. We use the algorithm described in Section 2, executed on a Silicon Graphics computer using 64-bit arithmetic with a relative convergence tolerance of 10^{-16} for all spatial moments.

The test problem considered here consists of an heterogeneous slab of width L= 0.1 meters. The left half has macroscopic total cross section $\sigma = 100\, m^{-1}$, c=0.5, with unit external source. The right half has $\sigma = 200\, m^{-1}$, c=0.05, and no source. It is solved using an S_4 Gaussian quadrature. We consider several uniform partitions, with h ranging from $L/2$ to $L/128$, and expansion orders Λ from zero to ten. In Fig. 1 we compare the first exact angular flux ψ_1^e to its approximations ψ_1 and $\tilde{\psi}_1$ calculated with h=$L/4$ (K=4) and Λ = 2. Part (a) of the figure shows the three fluxes, while Part (b) depicts the differences between the approximate fluxes and the exact solution. It is clear from the figure that $\underline{\psi}$ is significantly more accurate.

A quantitative assessment of accuracy can be obtained evaluating the L^2-norm of the error, i.e.

$$\varepsilon = \sqrt{\int_0^L \left| \underline{\psi}^e(x) - \underline{\psi}(x) \right|^2 dx} \quad , \qquad \tilde{\varepsilon} = \sqrt{\int_0^L \left| \underline{\psi}^e(x) - \underline{\tilde{\psi}}(x) \right|^2 dx}. \tag{18}$$

In Fig. 2 (a) we plot ε and $\tilde{\varepsilon}$ as functions of h for $\Lambda = 5$. The predicted asymptotic convergence orders are verified. Notice that the error in $\underline{\psi}$ is three orders of magnitude lower than that of $\underline{\tilde{\psi}}$ as soon as K is greater than 32. For coarser meshes, the difference is smaller, but for the full range ε is at least 20 times smaller than $\tilde{\varepsilon}$. Of most interest for the AHOT-N method is the capability of improving the accuracy by increasing the expansion order. Fig. 2 (b) plots ε and $\tilde{\varepsilon}$ as functions of Λ for $h = L/16$. Note that as Λ is increased by one the error decreases by a factor of ten. Also, ε is seen to be smaller than $\tilde{\varepsilon}$ by a factor that ranges from 10 (for $\Lambda = 0$) to 200 (for $\Lambda > 4$). The error indicator, η, plotted in Fig. 2 will be presented in Sec 5 below.

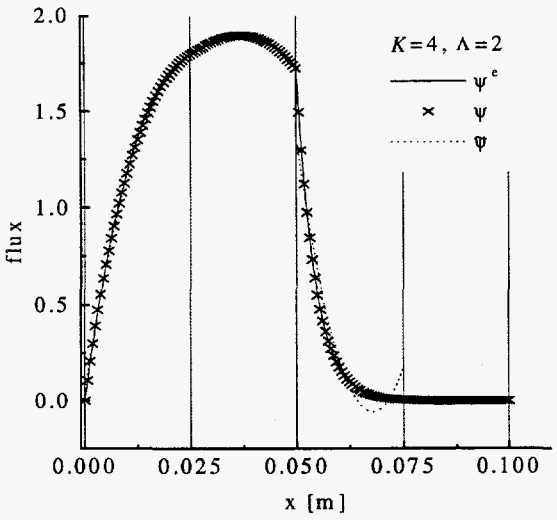

a) Angular fluxes for the K=4 case, Λ =2.

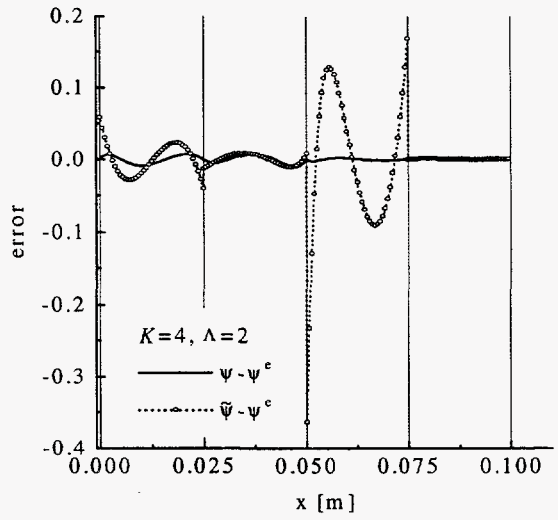

b) Differences between approximate fluxes and exact solution, K=4 case, Λ =2.

Figure 1. Relation between approximate fluxes and the exact solution for the K=4 case, Λ =2.

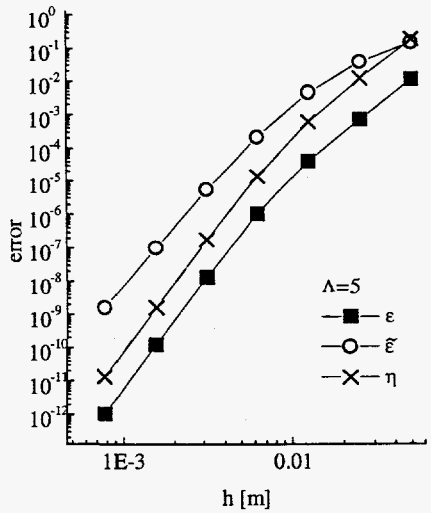

a) Errors ε and $\tilde{\varepsilon}$ as function of h for $\Lambda = 2$.

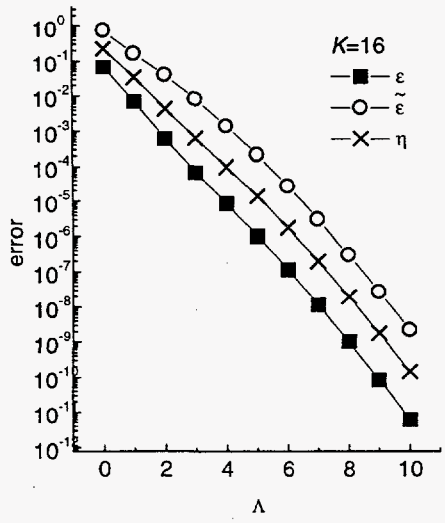

b) Errors ε and $\tilde{\varepsilon}$ as function of Λ

Figure 2. Errors of approximate solutions in L^2 norm.

4. Robust Form of the Spatial Weights Expression

The previous computations suffer from round-off instability when Λ is large. This is a consequence of Eq. 11, which can be rewritten as

$$\alpha_\Lambda(t_{i,k}) = \frac{\sum_{\lambda=\Lambda+1,even}^{\infty} e_\lambda(t_{i,k})}{\sum_{\lambda=\Lambda+1,odd}^{\infty} e_\lambda(t_{i,k})}, \tag{19}$$

From Eq. 19 it is clear that in the case of small cell optical thickness, $t_{i,k}$, or high Λ, both the numerator and the denominator in Eq. 11 tend to zero. To tackle this difficulty, asymptotic formulae were introduced (Azmy, 1998) which must be applied whenever the optical thickness is small. These formulae are incorporated into the code and the results employ them when necessary. They are

$$\alpha_\Lambda(t) \xrightarrow{t\to 0} \begin{cases} t/(2\Lambda+3), & \Lambda = 0,2,4,... \\ (2\Lambda+3)/t, & \Lambda = 1,3,5,... \end{cases} \tag{20}$$

This allows for the expansion order to be arbitrarily increased without suffering from pollution from finite-precision arithmetics.

5. *A Posteriori* Error Estimation

5.1 Error estimator and local error indicators

A posteriori error estimation is useful to estimate the accuracy of the solution for a given, completed, computation, and is most effective when used to refine the approximation to get maximal accuracy gain with minimal computing cost. Therefore an *a posteriori* error estimator must be an expression than can be easily evaluated using only the information obtained from the results of the numerical method. Let ε be defined as before, i.e., the true error of $\underline{\psi}$ measured in the L^2-norm. In Ref. (Zamonsky, 1999) it is shown that

$$\varepsilon \le \sqrt{\sum_k \frac{h_k^2}{2} \int_{x_{k-1/2}}^{x_{k+1/2}} \left(\underline{\underline{\mu}}^{-1} \left[\sigma_k \underline{\underline{S}}_k (\underline{\tilde{\psi}} - \underline{\psi})(x') + (\underline{\tilde{q}} - \underline{q})(x') \right] \right)^2 dx'} + h.o.t \equiv \eta + h.o.t. \tag{21}$$

where *h.o.t.* stands for "higher order terms". It is also shown that η preserves the order of ε, $O(h^{\Lambda+2})$. The crucial points are that η is computable, since it only depends on quantities that are known after the transport code is run, and that η estimates the true error (as it bounds it from above and converges to zero with the same order). This qualifies η as an *error estimator*.

Equation (21) estimates the global error throughout the computational domain. A natural question is how to refine the approximation so as to get maximal accuracy gain. The answer can be obtained via *local a posteriori error indicators*, which serve to indicate where the approximation should be refined to improve global accuracy at minimum expense. Let η_{ik} denote an error indicator for component i in cell C_k. By direct inspection, Eq. (21) can be rewritten as

$$\eta^2 = \sum_{i=1}^{N} \sum_{k=1}^{K} \eta_{ik}^2, \tag{22}$$

where

$$\eta_{ik}^2 \equiv \frac{h_k^2}{2}\int_{x_{k-1/2}}^{x_{k+1/2}} \left(\sigma_k \underline{\underline{\mu}}^{-1}\underline{\underline{S}}_k(\underline{\tilde{\psi}}-\underline{\psi})(x')+\underline{\underline{\mu}}^{-1}(\underline{\tilde{q}}-\underline{q})(x')\right)_i^2 dx', \tag{23}$$

so that, essentially, the estimator is the difference in scattering sources for direction i in C_k due to $\underline{\tilde{\psi}}$ and $\underline{\psi}$ plus $\underline{\tilde{q}}-\underline{q}$. This is natural in the sense that the truncation operation that defines the approximation acts only on the source (cf. Section 2). Consider the case in which the external source is exactly represented by $\underline{\tilde{q}}$, the error indicator for a non-scattering cell thus automatically vanishes. This should not be interpreted as the cell having zero error, which is false. The correct interpretation is that increasing the accuracy in the cell, by either splitting it into two or raising the order of the polynomial expansion, will not improve the solution accuracy.

For the case of isotropic scattering and if $\underline{\tilde{q}} = \underline{q}$, Eq. (23) further simplifies to

$$\eta_{ik}^2 = \frac{h_k^2}{2}\frac{\sigma_k^2 c_k^2}{\mu_i^2}\int_{C_k}\left(\tilde{\phi}-\phi\right)^2(x')dx', \tag{24}$$

where $\tilde{\phi}$ and ϕ are the scalar fluxes associated with $\tilde{\psi}$ and ψ, respectively, that, in the S_N approximation, are given by

$$\tilde{\phi} = \sum_{i=1}^{N} w_i\tilde{\psi}_i\ ,\ \phi = \sum_{i=1}^{N} w_i\psi_i\ . \tag{25}$$

Of most interest is an error indicator *per cell*, as it allows the identification of the cells in which large numerical errors are obtained. This is defined as

$$\eta_k^2 \equiv \sum_{i=1}^{N}\eta_{ik}^2\ , \tag{26}$$

which for isotropic scattering reduces to

$$\eta_k = \frac{\sigma_k c_k h_k}{\sqrt{2}}\sqrt{\int_{C_k}\left(\tilde{\phi}-\phi\right)^2(x')dx'}\sqrt{\sum_{i=1}^{N}\frac{1}{\mu_i^2}}\ . \tag{27}$$

5.2 Numerical tests

Numerical tests of *a posteriori* error estimators are aimed at showing that it behaves like the true error. In this case we address three types of behavior: The first, most classical, one, concerns the evolution of η as compared to ε as functions of h for fixed Λ. This is shown in Fig. 2 (a). The estimator correctly follows the error, showing that the higher order terms in Eq. 21 can in fact be disregarded. A second, less classical assessment, concerns the evolution of η with increasing Λ for fixed h. This is shown in Fig. 2 (b). The close resemblance of the curves corresponding to the estimator and the true error is remarkable. In fact, the theoretical analysis leading to Eq. 21 considers the limit $h \to 0$, so that the resemblance could not be predicted beforehand. To summarize, the results in Fig. 2 give us confidence that, when the approximation is refined by dividing cells or increasing the order, if the estimator decreases by some factor, the true error has also decreased by approximately the same factor.

For adaptivity purposes a third behavior is important, namely, for fixed h and Λ, the distribution of the estimated error over the various cells. This would allow improving the approximation only where it is most needed. In Fig. 3 (a) the true error and the local indicators are plotted for the same

numerical experiment as before, computed using 16 cells and an expansion order of 4. The same is done in Fig. 3 (b) for 64 cells and $\Lambda = 6$. Both graphs show that the local indicators follow closely the distribution of the true error over the domain. The most critical cell is identified as the one adjacent to $x=L/2$ from the right, and adaptive procedures using the proposed indicator would refine this region. By comparing Figs. 3 (a) and 3 (b), notice the already high accuracy of the computation with $h=L/16$ and $\Lambda = 4$, which is improved by about six orders of magnitude when $h=L/64$ and $\Lambda = 6$, though the number of computational unknowns has just increased by a factor of 6.

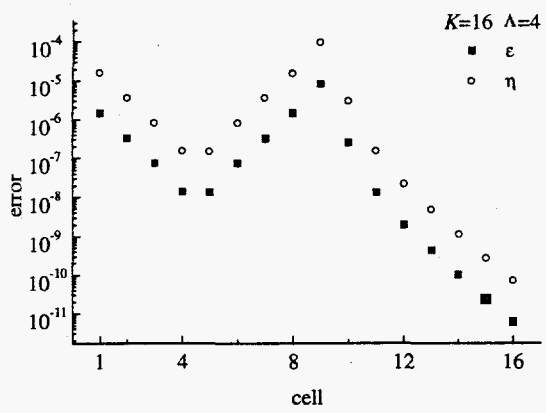

a) True error and indicator for the K=16 case, $\Lambda = 4$.

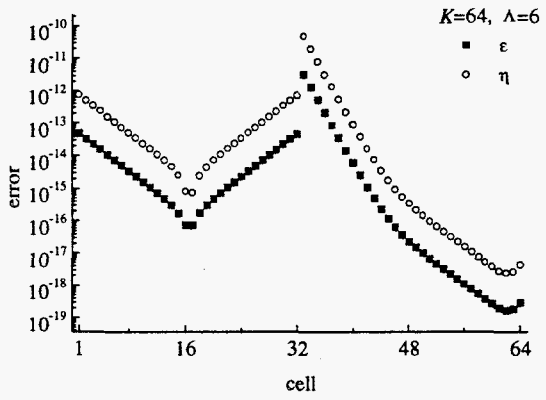

b) True error and indicator for the K=64 case, $\Lambda = 6$.

Figure 3. Behavior of the true error and indicator as function of the position.

6. Conclusions

Several numerical techniques aimed at improving and capitalizing the accuracy of the AHOT-N method have been developed and implemented. An assessment of these techniques on a strongly heterogeneous problem using S_4 Gaussian quadrature and several different cell sizes and expansion orders is reported. It confirms the proposed methodologies as leading to a robust, efficient and accurate computer implementation, with the possibility of automatic error control. Future work will be aimed at multidimensional problems and the design of adaptive criteria.

References

[Azmy, 1988] Azmy, Y. Y., The weighted Diamond-Difference Form of Nodal Transport Methods, Nucl. Sci. Eng., 29, 98, 1988.

[Azmy, 1998] Azmy, Y. Y., Zamonsky O. M., Thin-Cell Limit for the Spatial Weights of the Arbitrarily High Order Transport-Nodal Method, Proc. Am. Nuc. Soc., 130, 1998.

[Keller, 1988] Keller H. B. and Nelson P., Closed Linear One-Cell Functional Spatial Approximations: Consistency implies Convergence and Stability, Transport Theory and Statistical Physics, 191, 17, 1988.

[Nelson, 1987] Nelson P., Closed Linear One-Cell Functional Spatial Approximations, Ann. Nucl. En., 177, 1987.

[Victory, 1986] Victory, H. D. and Ganguly K., On Finite Difference Methods for Solving Discrete-Ordinates transport Equations, SIAM, J. Numer. Anal. 78, 23, No.2, 1986.

[Zamonsky, 1999] Zamonsky, O. M., Buscaglia, G. C. and Azmy, Y. Y., *A posteriori* error estimation for the One-Dimensional Arbitrarily High Order Transport-Nodal Method, to be published.